La mer 34: 215–225, 1996
Société franco-japonaise d'océanographie, Tokyo

ERS-1 SAR observations of dynamic features in the southern East-China Sea

L. M. MITNIK[1, 2], M. -K. HSU[1] and C. -T. LIU[3]

Abstract: ERS-1 SAR images covering the southern East-China Sea near Taiwan are analyzed together with relevant remote and *in situ* data to interpret the variations of their brightness (NRCS). A wealth of the oceanic and atmospheric phenomena of different scales were revealed on the SAR images: packets of internal waves, eddies and mushroom-like structures north and east of Taiwan, western Kuroshio front, natural and artificial slicks, island wakes, surface manifestations of bottom topography, cell and roll convection, atmospheric gravity waves, ets. Part of them had never been studied near Taiwan.

1. Introduction

The features of bottom topography in the southern part of the East-China Sea, vicinity of the vast Asia continent with full-flowing rivers, influence of Kuroshio, tide driven flows, indented coast line and coastal mountains disturbing wind field predetermine the complicated space-time structure of oceanic and atmospheric processes. Remote and *in situ* techniques, field and computer simulations are used to investigate these processes.

In spite of numerous efforts both the oceanic and atmospheric phenomena and processes are still not well known. This is particularly evident, when new devices and techniques are applied to study them. The primary attention in our research was concentrated on analysis of data obtained by a Synthetic Aperture Radar (SAR) from European ERS-1 satellite. Ground receiving station of the Center for Space and Remote Sensing Research at National Central University receives and processes the ERS-1 SAR images since October, 1993.

The active (different kinds of radars) and passive (radiometer) microwave techniques allow us to collect information about the ocean surface parameters and phenomena under cloud conditions. It is a great advantage for the areas where the probability of cloudiness is high. Radar images provide better resolution in comparison with microwave radiometric data. It allowed us to study the fine details of the oceanic phenomena. They manifest themselves as anomalous states of the sea surface as opposite to "normal" states when roughness is determined by surface wind only. Appearance of these states results from modulation of small scale wind waves by the variable currents directly and/or indirectly, for example, through redistribution of surface filmes. The atmospheric mesoscale phenomena (roll vortices, cell convection, gravity waves, wind shadows, etc.) are also imprinted in the surface roughness field due to modulation of horizontal surface wind.

The objective of this study is to interpret the brightness patterns observed on the ERS-1 SAR images collected over the southern East-China Sea to extract qualitative and quantitative information about phenomena in the ocean-atmosphere system. Processing of the SAR images and geographical distribution of the ERS-1 SAR-observed oceanic and atmospheric phenomena are described in section 2. Imprints of the roll vortices and the atmospheric gravity waves on the SAR images are considered in section 3. Surface manifestations of the Kuroshio front, upwelling, internal

[1] National Taiwan Ocean University, Keelung, Taiwan, R. O. C.
[2] Pacific Oceanological Institute, Vladivostok, Russia
[3] National Taiwan University, Taipei, Taiwan, R.O.C.

waves and other oceanic features are discussed in section 4.

2. Processing of SAR data. Map of dynamical phenomena

In image mode the SAR obtains strips of high resolution imagery approximately 100 km in width, 250 km to the right of the sub-satellite track. A spatial resolution is 26 m in range (across track) and between 6 m to 30 m in azimuth (along track) (VASS and BATTRICK, 1992). A SAR maps the surface roughness through Bragg scattering from the short gravity waves with a wavelength of $\Lambda = \lambda / (2\sin\theta)$, where λ is the wavelength of radar and θ is local incidence angle. ERS-1 SAR (λ =5.66 cm, θ = 19.5−26.6°, VV polarization) is sensivite to waves of about 8.3−6.5 cm long. For surface waves with crest at an angle ϕ to the radar line-of-sight, the Bragg scattering criterion is: $\Lambda' = \Lambda \sin \phi$. The differences in sea surface roughness are visible on the SAR images as tonal changes, with the light areas corresponding to stronger backscattering signals(to large values of normalized radar cross-section-NRCS). Backscatter increases with the increase of wind speed (stress) and depends on azimuthal angle (angle between wind vector and a plane of radar signal propagation). The threshold wind-speed value u_{min} needed to form the resonant Bragg waves depends on radar frequency and sea surface temperature and for ERS-1 SAR the $u_{min} \approx 3.2$m/s at a height of 10 m above the surface (DONELAN and PIERSON, 1987).

Each SAR frame covers an area of about 100 km by 100 km. The SAR data are in binary form. The digital SAR image had 8002 pixels in column and more than 8000 pixels in row. To enhance the features on a SAR image, decrease noise and achieve a convenient size, at first the size of the data was reduced by an 8×8 averaging box. A surface resolution of about 100 m resulting from this averaging was adequate for our study. Then the histogram of gray level was calculated and displayed. The upper and lower bounds of gray level were determined manually to provide the best visibility of the details. Image file was obtained by conversion of the binary file. Finally, the images ware printed by a laser printer using commercial image process package.

We analyzed about 150 ERS-1 SAR images obtained over southern part of the East-China Sea since October, 1993. These were both the individual images and strips of several images. Most of them covered the waters surrounding Taiwan between 21–27° N and 119–123° E. The images were obtained at different seasons and at different weather conditions. The NOAA AVHRR images, weather maps of the Japan Meteorological Agency (JMA) and the Central Weather Bureau, wave analysis map of the JMA and other relevant data were used to interpret the brightness variations on the SAR images and separate the oceanic phenomena.

Our analysis revealed, in particular, that the SAR images with the mesoscale (over a range several hundreds meters to several kilometers) wave-like variations of the surface roughness are wide spread and common. They can be caused by both the oceanic and atmospheric phenomena and can confuse an oceanographic interpretation of the SAR imagery. For instance, horizontal roll vortices, open and closed convective cells and gravity waves in the atmospheric planetary boundary layer produce the quasiperiodic surface-wind-speed (surface roughness) fluctuations. To detect an atomospheric nature of the observed organized NRCS variations, correlation of cloud patterns on the visible and/or NOAA images and brightness distribution on the SAR images was used. Furthermore, SAR images of oceanic internal waves which also produce the mesoscale modulation of the NRCS, look different from SAR images of wind rolls and atmospheric gravity waves (see below 4.3, as well as ALPERS and BRÜMMER, 1993; MITNIK and VIKTOROV, 1990; VACHON, *et al.*, 1994, 1995).

We marked the areas where the surface manifestations of the following phenomena were observed: the changes of bottom topography (BT), coastal fronts (CF), eddies (E), internal waves (IW), island wakes (IsW), Kuroshio front (KF), mushroom-like structures (MS), slicks (s), unusual ship wakes (SW), upwelling (U) as well as the surface imprints of cellular convection (CC), roll

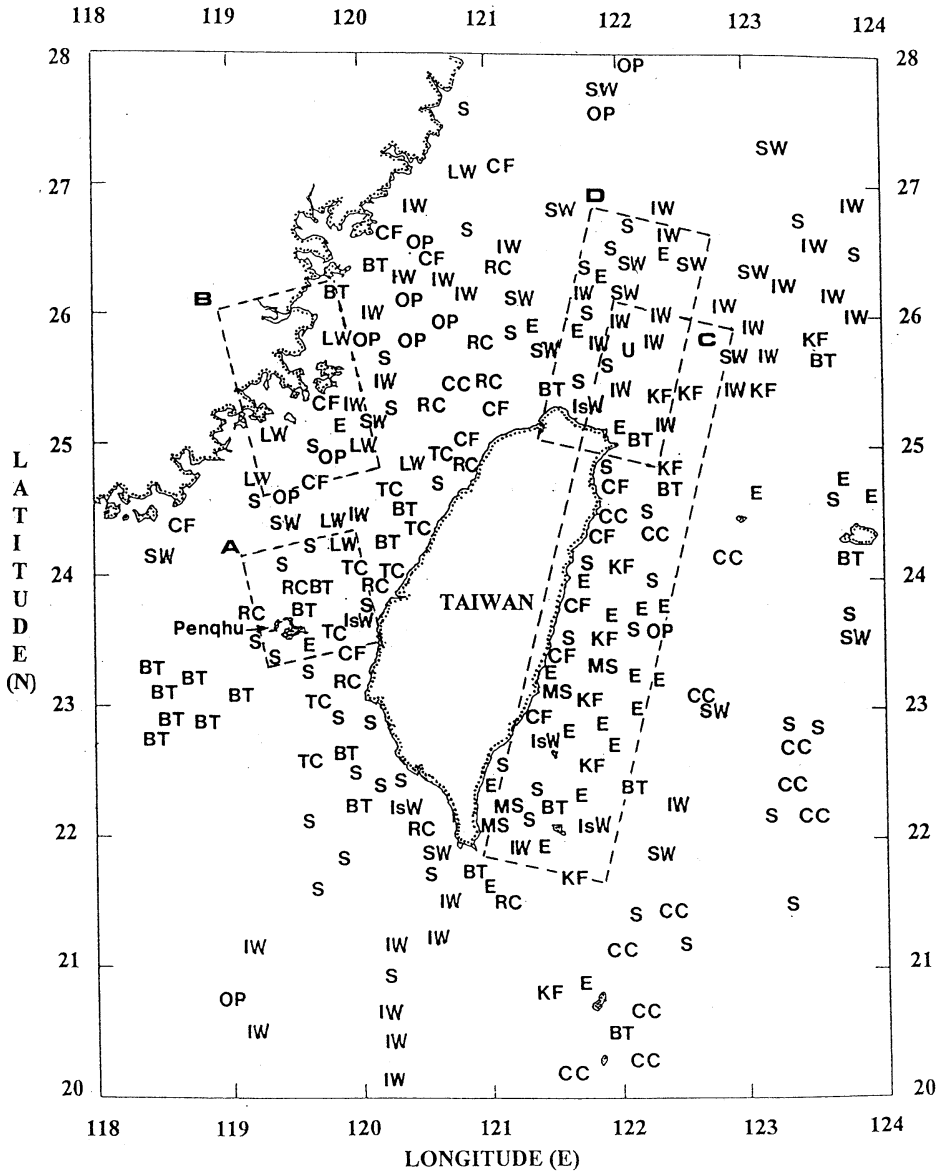

Fig. 1. Location of the features of sea surface roughness on the ERS-1 SAR images caused by the following oceanic and atmospheric phenomena near Taiwan: The changes of bottom topography (BT), coastal fronts (CF), eddies (E), internal waves (IW), island wakes (IsW), Kuroshio front (KF), mushroom-like structures (MS), slicks (S), unusual ship wakes (SW), upwelling (U), cellular convection (CC), roll convection (RC) and lee waves (LW). The dotted rectangles A, B, C and D show the locations of the SAR images used in the paper.

convection (RC) and lee waves (LW) (Figure 1). Several SAR strips were continued beyond the area under consideration. The mixed zone between Yangtze waters and waters of the East China Sea and internal waves in the Luzon Strait and in the northern South-China Sea were registered on them.

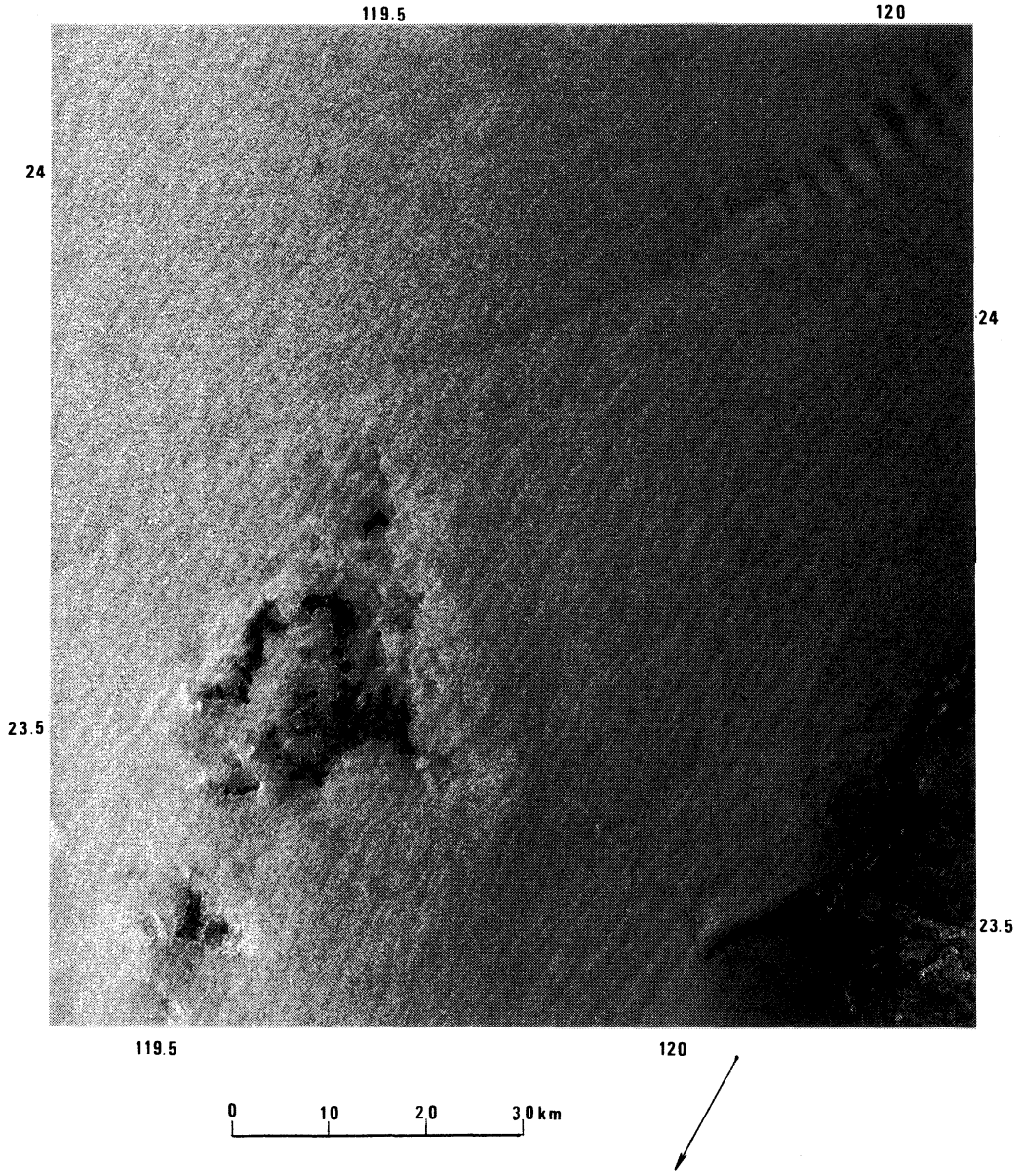

Fig. 2. ERS-1 SAR image of the Taiwan Strait, acquired on February 20, 1995, at 14 : 27 UTC (the original SAR image data is copyright ESA 1995). The image area is about 95 km x 100 km. Arrow shows mean wind direction derived from SAR image

3. Atmospheric phenomena

The oceanic phenomena can be detected with a SAR over a range of wind speed u from $u_{min} \approx 3.2$ m/s to 8–10 m/s only. At $u \geq 10$ m/s the brightness variations on a SAR image are mainly due to the sea surface wind variability. Figure 2 depicts a section of an SAR image teken over the Taiwan Strait near the Penghu (area A in Figure 1). From the weather maps of the JMA for 00 : 00 UTC on February 20 and 21, gale northeastern winds (prevailing during winter monsoon) and waves with a height of 3–4 m were observed at the time of the SAR pass. The increased brightness in the vicinity

of the Penghu was due to intensive wave breaking over shallow waters. It starts at a distance of about 8 km off northeastern coast. The boundaries of this area correlate well with isobaths and the results of Landasat image.

On the SAR image the alternating light and gray bands are surface expression of roll vortices in the marine boundary layer of the atmosphere. The surface waves that led to this streak-like pattern are formed primarily in response to variations in the surface wind caused by the rolls (ETLING and BROWN, 1993; ALPERS and BRÜMMER, 1993). The streak-like pattern has a mean orientation aligned with the north-northeastern wind (Figure 2). The distance between adjacent light lines determines a wavelenght of the roll vortices. It varies between about 1.5 and 2.5 km. The difference of the NRCS values of light and gray bands depends on wind speed of the base flow, amplitude of mesoscale circulation, azimuthal angle and incidence angle (MITNIK *et al.*, 1994).

Additionally to the roll vortices, the quasiperiodic variations of the NRCS can be resulted from atmospheric gravity waves. They are internal waves for which gravity is the restoring force (MITNIK and VIKTOROV, 1990; V ACHON, *et al.*, 1994; 1995). They modulate the horizontal surface wind speed and thus the surface roughness. A group of atmospheric gravity waves is seen in the upper right angle in Figure 2. Their wavelength is about 3.5 km and the wave crests are directed at a right angle to the bands, formed by the roll vortices.

At wind speed in the range of 3–10m/s the variations of the sea surface roughness (NRCS) are due to both the oceanic and atmospheric factors. A strip of two SAR images covering the East-China Sea east of China coast (Figure 3, area B in Figure 1) shows three systems of the surface imprints of the lee waves. In the system 1 20 well-defined wave crests of 2.7-km wavelength, in the system 2 9 crests of 4.3-km wavelength and in the system 3 8 crests of about 2.0 km wavelength are readily apparent in Figure 3. They are oriented near parallel to the coastal mountain ridges and extend up 40–50 km offshore. Modulation of the surface wind was enough to decrease u below a threshold value u_{min} needed to generate small gravity

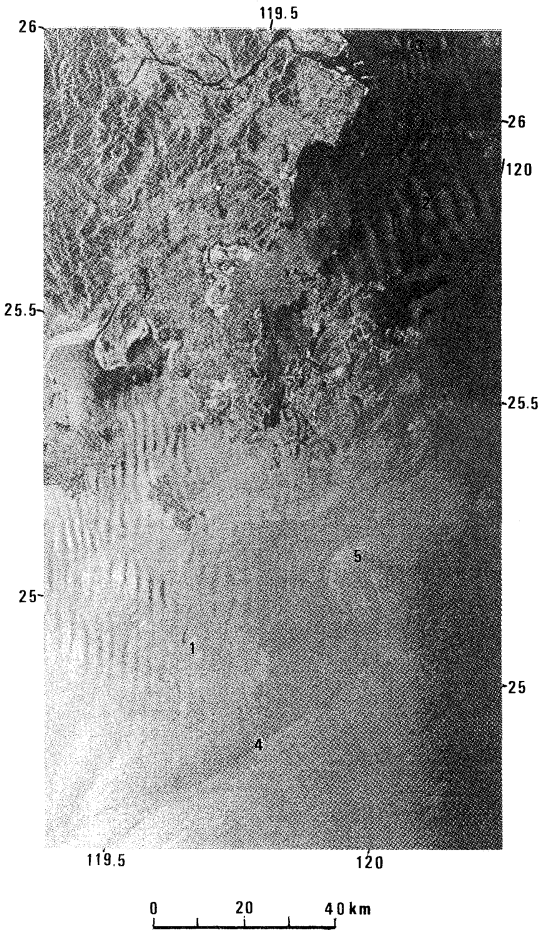

Fig. 3. ERS-1 SAR images of atmospheric lee waves east off China coast, acquired on December 8, 1994, at 14 : 26 UTC (the original SAR image data is copyright ESA 1994). The image area is about 100 km×160 km.

resonance waves with a wavelength of Λ. Amplitude of the modulation can be estimated with the CMOD IFR2 wind retrieval model for scatterometer (QUILFEN, 1995). From the model, it follows that the radar contrasts caused by the lee waves increase with the decrease of average wind speed.

A narrow contrast band 4 crossing part of the strip and ending by a cyclonic eddy 5 with size of about 10 km indicates, probably, a frontal boundary between the low-salinity China Coastal Current and the Taiwan Warm Current (GUAN, 1994).

4. Oceanic features

4.1 Kuroshio front

In the east Asia, the Kuroshio Current plays an important role in the local fishery, navigation and circulation. The season variations of the Kuroshio characteristics, such as location of axis, velocity, along-track width, flow separation, interaction with shelf of the East-China Sea, eddy formation, etc. are pronounced, especially northeast of Taiwan. These characteristics are studied with ships, drifters, NOAA AVHRR images, satellite altimeter data and computer simulation. The short time variability of the Kuroshio was explored to a significantly lesser degree. Only NOAA AVHRR images can cover the Kuroshio and surronding waters, as opposite to altimeter and *in situ* measurements. However, a high probability of cloudiness coupled with thermal contrasts of the Kuroshio waters against a background in the area under consideration do not allow to use the IR images which proved to be a very effective in Kuroshio study east of Japan. The possibility of imaging radars to detect the dynamic phenomena can help us to understand better behavior of the Kuroshio front and, in particular, to clarify the main causes of its variability.

A strip of five SAR images obtained on April 23, 1995 covers a region approximately 100 km by 500 km off the east coast of Taiwan (Figure 4a, area C in Figure 1). The individual frames are marked by digits 1–5; the dotted lines show boundaries between them (Figure 4b). The SAR images of the same Kuroshio area were also acquired on November 26, 1993; May 28, July 2 and August 6, 1995. The coastal mountains and valleys are seen along the left-hand boundary of the strip. The strip is essentially an instant pattern showing surface expressions of interaction of northward Kuro-shio flow with bottom topography and islands east of Taiwan coast. The complicated structure of the Kuroshio front is clear visible on the strip. The bright and dark bands of varying width represent the frontal boundary of the Kuroshio (Figure 4b). They are aligned parallel to the coast about 40–50 km away from it. It is suggested that the increased values of the NRCS (bright bands) are due to short gravity-wave/current interaction along shear and/or convergence zones within the front. The reduced valued of the NRCS (dark bands) are due to increased concentration of natural surface films aligned along frontal boundary (MARMORINO *et al.*, 1994; NILSSON and TILDESLEY, 1995; VESECKY and STEWART, 1982).

Cold front was north of Taiwan at approximately 27° N. It shifted to the south at the time of the SAR pass. Southerly winds of about 5–7 m/s and air temperature of 27–28℃ were recorded by the coastal station at 24° 20′ N, 123° 45′ E (the JMA surface analysis at 00: 00 and 00: 06 UTC) and the JMA wave analysis map at 00: 00 UTC (2.5 h before the SAR pass). Northward wind wave height was 1 m and westward swell height was 2 m and northward wind of 5 m/s were reported by ship at 24° N, 128° 30′ E. In accordance with ten-day mean sea surface temperature (SST) of the JMA, the SST was 27℃ south of 24° N. It decreased to 25 ℃ near 26° N. In the NOAA-12 IR image for April 24 processed by the Fishery Research Institute, Keelung, the SST decreases from 29℃ south of Taiwan to 27℃ at about 23–24° N. Lack of *in situ* observation of atmospheric parameters hinders, however, the estimate of influence of the wind stress variations induced by the changes of atmosphere stability on radar contrast.

Eddy-like and wave-like disturbances of the boundary are caused by interaction of Kuroshio with islands, underwater ridges and mountains. Island wake was formed behind Lutao (frame 4). A shape of the individual eddies downstream Lutao was perturbed by current shift. Further north, an underwater mountain at about 23° 30′, 121° 48′ is a cause of the increased surface roughness (frame 3). The area over another bottom raising near 24° 40′, 122° 20′ is also characterized by increased backs-catter (frame 2). North of this area the Kuroshio waters turn northeast. The small-scale linear striations north of the raising and around the right side of the boundary between the 1st and the 2nd frames are, probably, the surface effects of the adjustment of the bottom boundary layer to the changes in the interior flow. The similar SAR signatures were observed in the eastward deflection zone of the

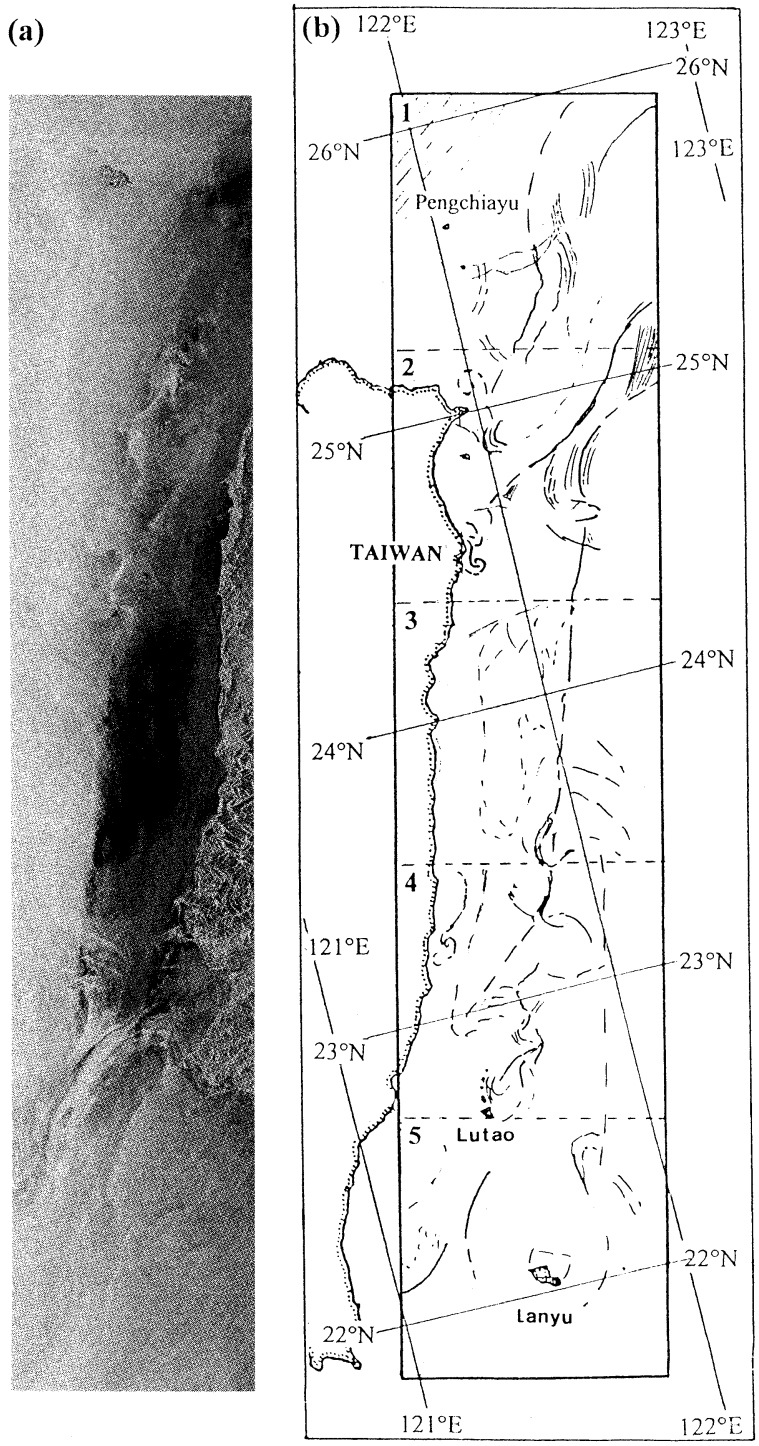

Fig. 4. SAR strip of five frames from ERS-1 on April 23, 1995, at 02 : 37 UTC (the original SAR image data is copyright ESA 1995) (a) and free-hand drawing of the contrast features (b), showing Kuroshio front, eddy-like structures along the front, packets of internal waves and surface manifestations of bottom topography.

Gulf Stream (FU and HOLT, 1982). Interaction of Kuroshio and tidal currents with shelf break causes generation of internal wave (IW) propagating both offshore and onshore (frame 1).

On the SAR images of Kuroshio acquired on other dates, several eddy-like structures behing Lanyu and Lutao as well as spiral eddies between these islands and over the underwater mountain at 23°30′, 121°48′ were observed. The possibility of eddy formation for currents flowing over topographic features was investigated theoretically by HUPPERT and BRYAN (1976). Intensive packets of the IW were observed in the area of frame 1 and further northeast. Their crests were directed approximately parallel to isobaths.

4.2 Upwelling

The region northeast of Taiwan is a region of the interaction between the Kuroshio and the East-China Sea waters. Satellite and ship observations were used to study upwelling (cold eddy) and the change of the western Kuroshio boundary in this area (CHEN, 1994; LIN, 1992). The upwelling was detected on Almaz-1 and ERS-1 SAR images as the area of reduced backscatter since 1992 (LIU *et al.*, 1992; HSU *et al.*, 1995).

Outlines of a large dark patch and the smaller dark features north of it on the SAR images (Figure 5, area D in Figure 1) agree with cold waters determined by NOAA-11 AVHRR (HSU *et al.*, 1995). The decrease of the SST was about 1–4℃. The cold waters are the upwelled subsurface nutrient-rich Kuroshio waters which impinge on the shelf break northeast off Taiwan. Damping of small scale roughness in this area may be caused by an increased surface film concentration and viscosity of slick-covered waters and by the more stable boundary layer of the atmosphere. Ship data collected during the Kuroshio Edge Exchange Program confirm both the SST decrease and the increased concentration of phytoplankton in the area of upwelling.

The scale, configuration, SST contrast and concentration of films vary here with time. Usage of SAR data can improve monitoring of upwelling. From the sequence of 23 SAR passes, collected in 1992–1995, evidence of upwelling expressions assumed to be caused by the increased film concentration were cleary identified in 14 scenes out of 20 implying a capture rate of about 60%. During these 14 SAR overpasses the wind speed was between 2–3 and 10 m/s. The SAR images (Fig. 5) were taken at wind speed of 2-5 m/s. Swell with a wavelength of about 290 m from the strong tropical storm Walt with the center at 29.8° N, 133° E (1200km northeast of Taiwan) is cleary visible on the image.

4.3 Internal waves and eddies

Numerous packets of internal waves resulted from interaction of tidal current with the shelf break north of Taiwan were detected on the SAR images (Figure 1). Surface manifestations of several groups of the IW propagating to the east (at an almost right angle to swell) can be distinguished in Figure 5 a. The crest lines are curved and their lenghts decrease from the front to the rear. Their wavelenghts decreased too due to the decrease of the amplitudes of the successive waves. The leading wave of a packet crossing the northeastern boundary of the dark patch has a large intensity: it is visible in the slick area due to surface wave breaking.

28 SAR images were collected in the southern East-China Sea. The packets of the IW propagating both offshore and onshore with an average group velocity of about 0.3–0.7 m/s were detected on 19 frames obtained at various environmental and tide conditions. A high probability of the IW detection denotes that the IW are a common phenomenum in the considered area. (The estimates of group velocity were obtained by measurements of the distance between packets of the IW identified in a particular SAR image. Analysis of the shape and the location of the packets allowed us to suggest that the packets were generated in the same sources by successive semidiurnal tidal cycles).

Eddies usually show up in SAR images as a result of wave/current interaction, which outlines the curved shape of the eddy, or are revealed indirectly through the presence of natural film trapped within spiraling lines associated with the eddy's orbital motion. The eddy having a large thermal contrast against a

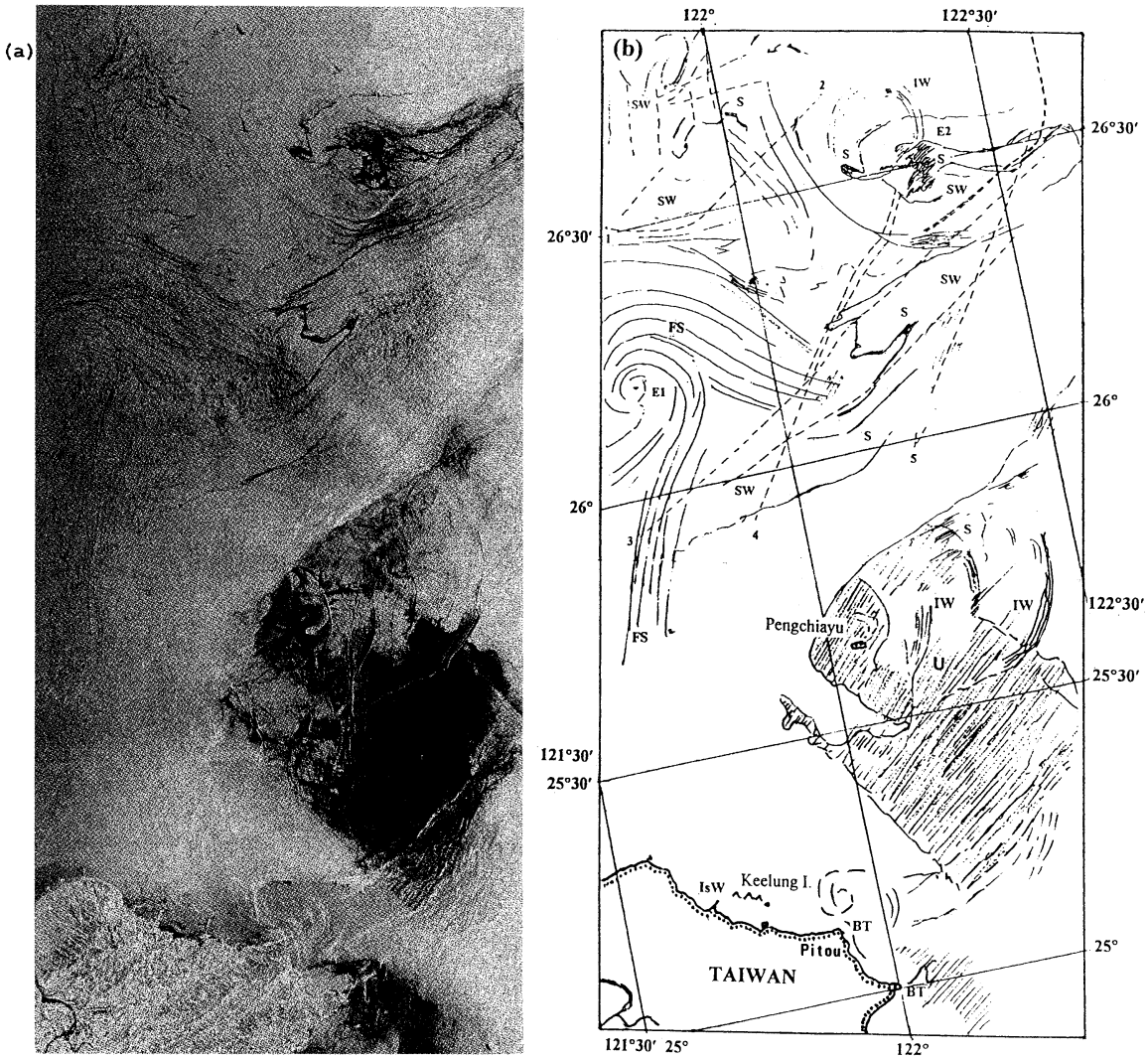

Fig. 5. SAR strip of two frames from ERS-1 on July 23, 1994, at 02 : 26 UTC (the original SAR image data is copyright ESA 1995) (a) and free-hand drawing (b), showing the location of upwelling (U), internal waves (IW), eddies (E1, E2), slicks (S), filamentaly slicks (FS), surface manifestation of bottom topography (BT), island wake (IsW) and ship wakes (SW); ---- turbulent ship wake, ====-bright turbulent ship wake; 1–5–ships.

background can also be expressed by the change in wind stress across the temperature front (LICHY *et al.*, 1981; MITNIK and LOBANOV, 1991).

Mesoscale eddies E1 and E2 are made apparent in the SAR images by embedded narrow natural slicks (Figures 5a and 5b). These filamentary slicks (FS) aligned in spiral configuration reveal the E1 eddy. The spiral lines suggest convergence towards the eddy center. Concentration of natural surfactants is higher in the area of the E2 eddy. The decreased SST (about 1–3℃) identifies this area in the IR image (HSU *et al.*, 1995).

The variations of backscatter near Taiwan coast result from interaction of tidal current with the features of bottom topography (BT). A small-scale spiral eddy is seen north of Cape Pitou. An island wake (IsW) west of Keelung Island indicates the direction of the tidal

current (Figures 5).

5. Conclusion

This study has shown that under moderate (3–10 m/s) and strong (>10 m/s) winds the SAR can detect the imprints of the organized mesoscale structures in a field of horizontal sea surface wind caused by the wave phenomena in the boundary layer of the atmosphere: roll vortices, atmospheric gravity waves, etc. At high sea states the increased wave breaking (and thus, the increased values of the NRCS) marks the boundaries of the shallow waters.

Various oceanic phenomena manifest themselves under moderate winds only. These manifestations can have both positive and negative radar contrasts relative to the background. The narrow curved bright features sometimes in conjunction with the stretched slick bands and filamentary slicks allow to detect Kuroshio front, eddies of different sizes, mushroom-like currents, packets of internal waves, coastal fronts, etc. The upwelling north of Taiwan looks dark, likely, due to the increased concentration of natural surface films damping short gravity waves. The bright features arranging themselves into wave-like or eddy-like structures are also resulted from interaction of currents with underwater relief, islands and headlands.

These preliminary results demonstrated the potential of a satellite SAR for detecting and studying dynamical phenomena both in the atmosphere and in the ocean. With regular access to SAR observations, understanding of complex processes in air/sea system will be improved, especially in coastal region.

Acknowledgments

We thank the European Space Agency for ERS-1 and the staff at ESRIN and the Center for Space and Remote Sensing Research at National Central University in Taiwan for their enthusiastic help in data acquisition and processing. We are grateful to Maia Mitnik for figures' preparation and S. S. Yu and S.-C. Huang for assistance in processing of SAR images. This research was sponsored by the National Science Council through research grants NSC-82-0209-M002a-046W, NSC-83-0209-M019-010 and NSC-84-2611-M019-009.

References

Alpers, W. and B. Brümmer (1994): Atmospheric boundary layer rolls observed by the synthetic aperture radar aboard the ERS-1 satellite. J. Geophys. Res., **99**, 12613–12621.

Chen, Y.-L. L. (1994): The importance of temperature and nitrate to the distribution of phytoplankton in the Kuroshio-induced upwelling northeast of Taiwan. Proc. National Science Council, ROC. Part B: Life Sciences., **18**, 44–51.

Donelan, M. and W. Pierson (1987): Radar scattering and equilibrium ranges in wind-generated waves with applications to scatterometry. J. Geophys. Res., **92**, 4971–5029.

Etling, D. and R. A. Brown (1993): Roll vortices in the planetary boundary layer: a review. Bound.-Layer Meteor., **65**, 215–248.

Fu, L.-L. and B. Holt (1982): Seasat Views Oceans and Sea Ice with Synthetic Aperture Radar. JPL Publication 81–120, 200pp.

Hsu, M.-K., L. M. Mitnik and C.-T. Liu (1995): Upwelling area northeast of Taiwan on ERS-1 SAR images. Acta Oceanographica Taiwanica, **34**, 27–38.

Huppert, N. E. and K. Bryan (1976): Topographically generated eddies. Deep-Sea Res., **23**, 655–679.

Lichy, D. E., M. G. Mattie and L. J. Mancini (1981): Tracking of a warm water ring. *In*: Spaceborne Synthetic Aperture Radar for Oceanography, Beal, R. C. P. S. DeLeonibus and I. Katz, (eds.), Johns Hopkins University Press, Baltimore, Md., 215pp.

Lin, C.-Y., C.-Z. Shyu and W.-H. Shih (1992): The Kuroshio fronts and cold eddies off northeastern Taiwan observed NOAA AVHRR imageries. Terrestrial, Atmospheric and Oceanic Sciences (TAO), **3**, 225–242.

Liu, C.-T., L. M. Mitnik, M.-K. Hsu and Y.Yang (1994): Oceanic phenomena northeast of Taiwan from ALMAZ SAR image. TAO, **5**, 557–571.

Marmorino, G. O., R. W. Jansen, G. R. Valenzuela, C. L. Trump. J. S. Lee and J. A. C. Kaiser (1994): Gulf Stream surface convergence imaged by synthetic aperture radar. J. Geophys. Res., **99**, 18315 18328.

Mitnik, L. M., C. -T. Liu, M. -K. Hsu and K. S. Chen (1994): Mesoscale atmospheric organized structures over the Asian marginal seas on satellite radar images. Preprints of Second Intern. Conference on Air-Sea Interaction and on Meteorology and Oceanography of the Coastal Zone. Lisbon, Portugal, 22-27 September 1994, 175.

MITNIK, L. M. and V. B. LOBANOV (1991): Reflection of the oceanic fronts on the satellite radar images. *In*: Oceanography of Asian Marginal Seas, Takano, K. (ed.), Elsevier Oceanography Series, **54**, Elsevier, Amsterdam, P.85–101.

MITNIK, L. M. and S. V. VIKTOROV (ed.) (1990) Radiolokatsiya Poverkhnosti Zemli iz Kosmosa (Radar Imaging the Earth's Surface from Space). Gidrometeoizdat, Leningrad, 200 pp. (in Russian).

NILSSON, C. S. and P. C. TILDESLEY (1995): Imaging of the oceanic features by ERS 1 synthetic aperture radar. J. Geophys. Res., **100**, 953–967.

QUILFEN, Y. (1995): ERS-1 off-line wind scatterometer products. CERSAT, Ref.: C1-EX-MUT-CD0000-03-IF, 58 pp.

VACHON, P.W., O.M. JOHANNESSEN and J.A. JOHANNESSEN (1994): An ERS 1 synthetic aperture radar image of atmospheric lee waves. J. Geophys. Res., **99**, 22483–22490.

VACHON, P. W., J. A. JOHANNESSEN and D. P. BROWNE (1995): ERS-1 images of atmospheric gravity waves. IEEE Trans. Geosci. Remote Sensing, **33**, 1014–1025.

VASS, P. and B. BATTRICK (eds.), (1992): ERS-1 System ESA SP-1146, ESA Publications Division, c/o ESTES, Noordwijk, The Netherlands, 87 pp.

VESECKY, J. and R. STEWART (1982): The observation of ocean surface phenomena using imagery from the SEASAT SAR: an assessment. J. Geophys. Res., **87**, 3397–3430.

Received January 13, 1996
Accepted March 8, 1996